

# NFAL Prototype Design and Feasibility Analysis for Self-Levitated Conveying

Xiaoni Chang<sup>1</sup>, Bin Wei<sup>2\*</sup>, Mark Atherton<sup>3</sup>, Cris Mares<sup>3</sup>, Tadeusz Stolarski<sup>3</sup>, Ahmed Almurshedi<sup>3</sup>

*1 School of Economic and Management, Beihang University, Beijing, China, 100191*

*2 State Key Laboratory of Tribology, Tsinghua University, Beijing, China 100084*

*3. College of Engineering, Design and Physical Sciences, Brunel University London, UK*

*4. National Key Laboratory of Vehicle Transmission, China North Vehicle Research Institute, Beijing 100072, China*

**Abstract:** In order to avoid friction and scratching when conveying objects, a squeeze-film levitation prototype was designed to verify the feasibility. The modal shapes and the forced harmonic shapes of the prototype are obtained by an ANSYS coupled field computation with a  $\frac{1}{4}$  symmetry model and the levitation capacity was assessed by the use of groups of simulation and physical testing. The simulation results show that the pure flexural and mixed flexural wave shapes with different wave number exist at specific frequencies. The amplitude of the central point of an aluminium plate having four piezo-electric discs glued to the bottom surface was simulated for a frequency spectrum. The experimental results confirm the theoretical results and the feasibility of the prototype, and also confirm that objects can be floated at several resonant frequencies under forced vibration conditions. The system provides the largest levitating capacity when both the piezo-electric disc and the plate resonances coincide.

**Keywords:** NFAL; ANSYS; Prototype; Resonant; Piezoelectric; squeeze-film levitation

## 1 Introduction

The Near Field Acoustic Levitation (NFAL) or squeeze-film levitation concept comes from high frequency gas squeeze theory. The gas squeeze theory is originally proposed by Gross<sup>[1]</sup> and improved by Langlois<sup>[2]</sup>. Next, Salbu<sup>[3]</sup> proposed the fixed object squeeze film model and believed that the squeeze film characteristic is similar to a piston-excitation situation. The carrying capacity can be obtained by simple calculation. Free levitation theory was first proposed by Beck<sup>[4]</sup> and a numerical method is applied in his model. Later research on squeeze film characteristics was addressed by lubrication dynamic methods developed over more than 20 years<sup>[5,6]</sup>. Based on free levitation theory, the modal

---

\* Corresponding author

shapes were considered in Hashimoto's research<sup>[7]</sup>. The excited shape was assumed to be an ideal flexural wave and coupled to the film thickness equation. The model proved to be more stable and a higher load capacity than that in the rigid disc excitation condition. Later, a linearisation solution was derived by Minikes and Bucher<sup>[8]</sup> and the feasibility was verified by Hashimoto's experimental results. Stolarski and Chai investigated the characteristics of the designed linear bearing from which the 2D model for the new bearing was gradually established<sup>[9,10]</sup>. Li et al<sup>[11,12]</sup> researched the bearing force through experiments and plotted the film thickness versus frequency curves. Recently, some scholars combined squeeze film theory with ultrasonic phenomenon<sup>[13]-[16]</sup> and compared the ultrasonic levitation results with squeeze film by numerical computation. Thus the concept of an 'ultrasonic squeeze film' was proposed and the theory was further developed. Recently, from the point of view of engineering practice, researchers focus on specific situations of the squeeze film such as the Non-Newtonian fluid film, the film with porous layer and damping effects<sup>[17]-[19]</sup>.

Research history for Near Field Acoustic Levitation (NFAL) is listed in Tab.1., showing different models and solution methods for the NFAL system. There are three main models for the NFAL system; they are infinite width model for simply estimating, axial symmetry model for the round exciting disc and 2-D model for a common exciting plate. All of the modal shapes, including rigid, pure flexible, mixed (true) models and object status could influence the complex extent of the mathematic models. The solutions corresponding to the models mainly included acoustic radial field and squeeze film methods, however, for the free object the model can only be solved by numerical methods.

In engineering practice, the piezoelectric horn is an effective actuator design<sup>[20]</sup>. However, due to space constraints, the horn cannot be used in a self-levitation conveyor system. For a flat plate design actuated by piezo discs, the resonance frequency of the system is difficult to predict and greatly affected by the layout of the piezo-discs.

Tab.1 The research history of the NFAL

Publication Time	First Author	Model Type	Modal Shape of Excitation Disc	Sample suspended situation	Calculation method
1961	Langlois <sup>[2]</sup>	Infinite Wide Axial Symmetry	Not take account	Fixed	Reynolds equation perturbation
1964	Sablu <sup>[3]</sup>	Axial Symmetry	Not take account	Fixed	Reynolds equation numerical method
1968	Diprima <sup>[21]</sup>	Infinite Wide	Not take account	Fixed	Reynolds equation analytic method

1969	Beck <sup>[4]</sup>	Axial Symmetry	Not take account	Free	Reynolds equation and motion equation perturbation method
1983	Takada <sup>[22]</sup>	Infinite Wide	Not take account	Fixed	Reynolds equation linearization method
1984	.Kuroda <sup>[23]</sup>	Axial Symmetry	Not take account	Free	Numerical method
1996	.Hashimoto <sup>[7]</sup>	Infinite Wide	Flexible modal shape	Fixed	Ultrasonic analytical theory
1997	Beltman <sup>[24]</sup>	2D Rectangle	Not take account	Fixed	Finite element method
2003	Butcher <sup>[25]</sup>	Axial Symmetry	Flexible modal shape	Fixed	Numerical method
2004	Minikes <sup>[8]</sup>	Infinite Wide	Rigid and Flexible model	Fixed	Modified Reynolds linearization method
2006	Stolarski <sup>[9]</sup>	2D Model	Not take account	Fixed	Reynolds equation numerical method
2006	Stolarski <sup>[27]21</sup>	2D Model	Flextrual model	Fixed	Experiment reserch
2007	Yoshimoto <sup>[27]</sup>	2D Model	Take account	Free	Reynolds equation numerical method ANSYS fluid simulation
2009	Liu <sup>[11]</sup>	Axial Symmetry	Flexible Wave	Fixed	Reynolds equation numerical method
2010	Stolarski <sup>[10]</sup>	2D Model	Take account	Free	Reynolds equation numerical method ANSYS fluid simulation
2011	Wei <sup>[28]</sup>	Axial Symmetry	Real modal shape	Fixed	ANSYS ultrasonic simulation
2012	Stolarski <sup>[29]</sup>	2D Model	take account	Fixed	Reynolds equation numerical method
2014	Wei <sup>[20]</sup>	Axial Symmetry	Mixed modal shape	Free	Reynolds equation analytic and numerical method
2014	Wei <sup>[22]</sup>	Infinite wide	Rigid model	Fixed	Reynolds equation linearization method

---

## 2 Prototype Design

The physical NFAL platform and the levitated samples are shown in Fig.1. The dimension and the materials of the piezo-electric discs and the exciting plate are listed in Tab.2. The four piezo-electric discs are connected with the output port of the amplifier by the block terminal with a 1-Amp fuse. The layout of piezo-electric discs is shown in Fig.2.

The piezo-electric discs are fixed at the bottom of the plate with professional adhesive, and then subject to a distress treatment for 12 hours. Therefore, the prototype of the actuator (exciting plate) is made up of the plate and the piezo-electric discs which can squeeze the gas which is close to the plate surface. In this circuit, the capacitances are parallel connected, and resonant frequency is determined by the total capacitances and equivalent inductances. The system resonance frequency and impedance are more important to the levitation capacity than the individual properties of the piezoelectric discs. Several metallic and non-metallic sample objects, shown in Fig. 3, were chosen to test the levitation effects in the experiment. The plate actuator design is detailed in Fig.2.

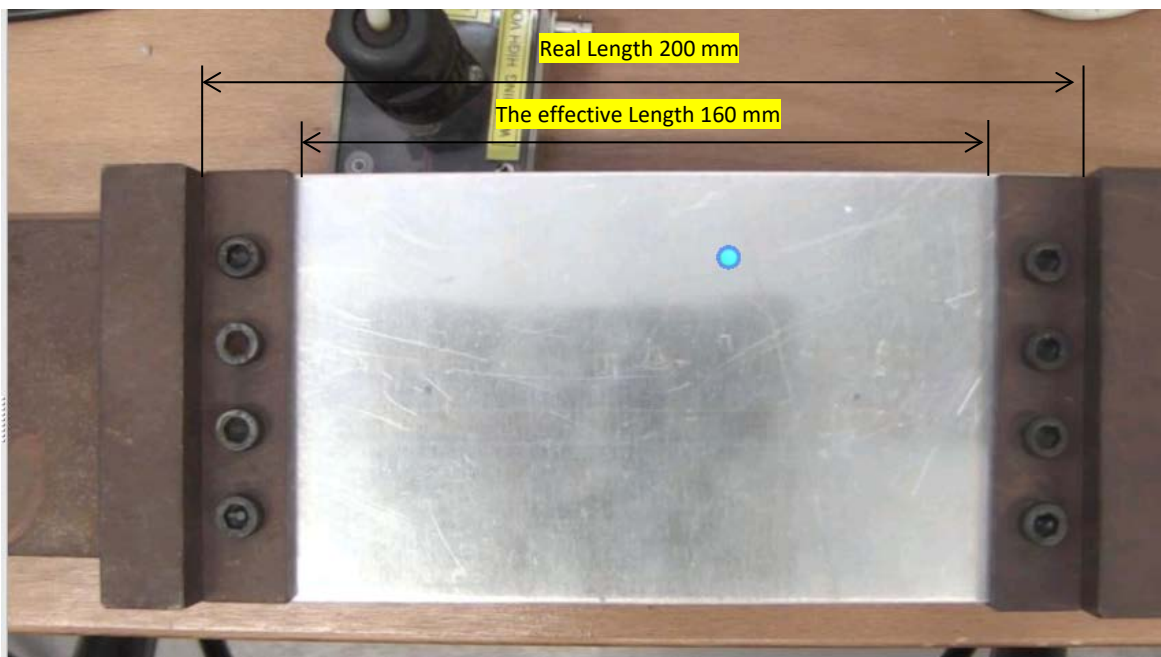


Fig.1 The designed plate actuator

Tab.2 Dimensions and materials of the piezo-electric discs and the plate

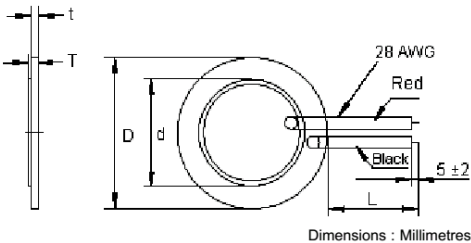
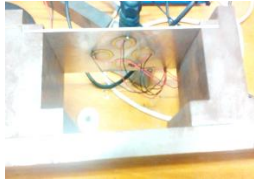
Sort	image	Drawing	Properties
Piezo-electric disc			<p>Materials: Brass and iron</p> <p>Resonant frequency: 4.2K</p> <p>D:27mm</p> <p>d: 20mm</p> <p>t=0.3</p> <p>T=0.5</p>

Plate and layout



As Fig.2

Materials: Aluminium

Real length:200mm

Effective length:160mm

Width:100mm

Height:2mm

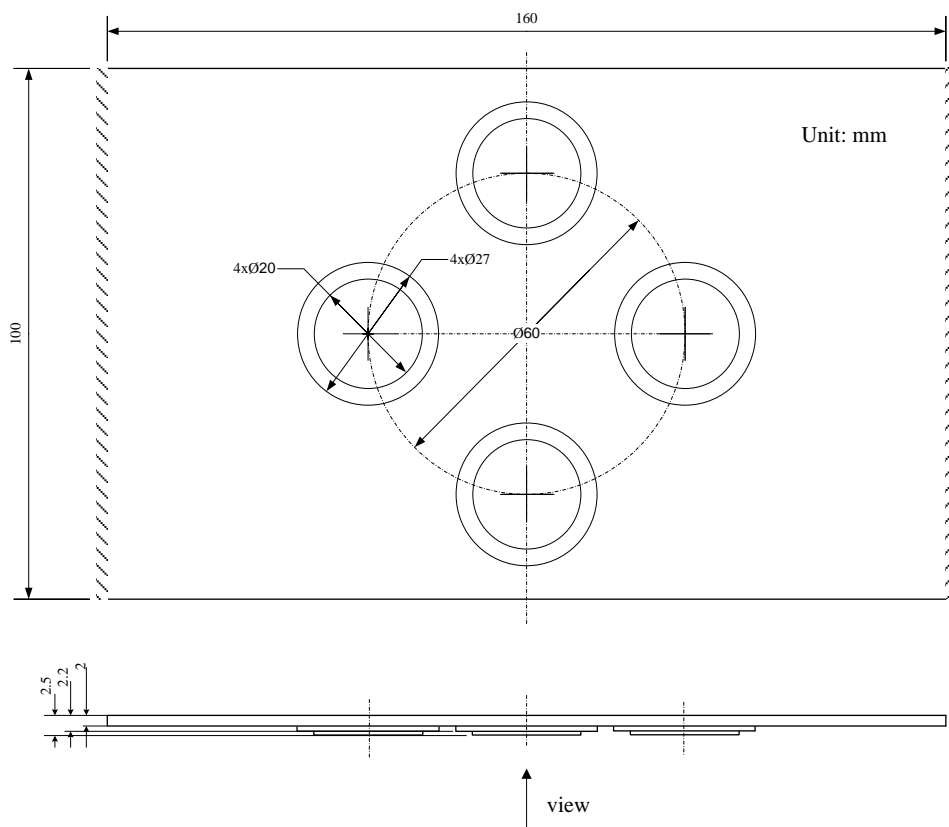


Fig.2 Dimension of the exciting plate



Fig.3 Levitation samples.

### 3. The plate finite element and the squeeze film model of the piezoelectric plate actuator

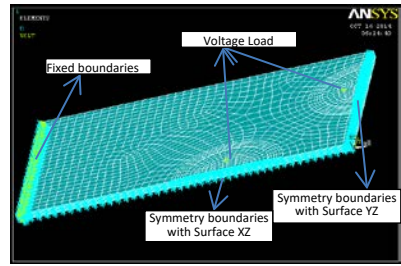
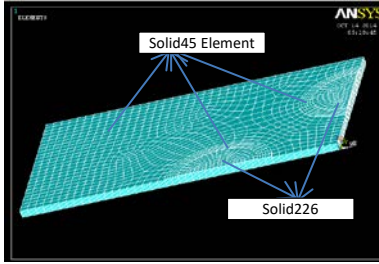
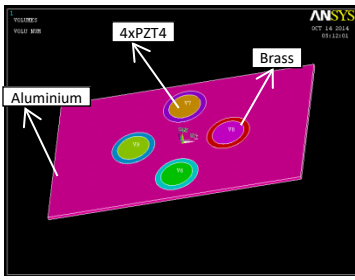
As the air pressure boundary condition is omitted in the Finite Element Mesh (FEM) model of the exciting plate, it is reasonable to calculate the modal and harmonic shapes first, and then obtain the film thickness equations by coupling with the plate shapes, from which the bearing force (pressures at nodes) are calculated using the Reynolds equation coupled with the film thickness equation.

#### 3.1 The Finite element model of the exciting plate

The deforming shapes of the plate actuator can be determined from the FEM model. The mathematical model is determined by the geometric dimensions of the plate and the piezoelectric discs (Fig.2). The FEM vibration model for PZT-4 was researched theoretically and experimentally and was found to be adequate when compared to the results of disc excitation experiments [20]. The FEM model and boundary condition of the exciting plate are shown in Tab.3. The materials parameters are listed in Tab.4. The model coupled with electric-structure would be preferred for simulating the real experiment status. Three materials are included, that is aluminium plate, brass linings and PZT4 actuators, which are glued to each other in the ANSYS Pre-treatment. In engineering practice, the symmetry modal shapes (either with XZ or YZ plane) are available to ensure the objects are able to steadily self-levitate in the central area on the conveyor belt. So, only a quarter of the geometry is meshed due to the symmetry structure, by which, some of the irregular modes would be missed, but it is possible to extract the main modes from the multiplex ones. The model is divided into different partitions to ensure the hexahedral mesh by the sweeping method. There boundary conditions applied to this model are fixed boundaries on the left side of the plate, symmetry boundaries on the XZ and YZ Plane and 75 Volt difference on the each side of the piezo-electric disc. The static modes and harmonic results of the disc can be obtained by the ANSYS electric-structure-coupling analysis.

Tab.3 The Finite model and boundary condition of the exciting plate

Geometry and materials	Hexahedral mesh and element	Boundary condition and Load
	(1/4)	(1/4)



The key Input parameters for the metal and PZT materials are listed in Tab.4

Tab.4 The materials of the elements.

Materials	Dielectric constants	Young's	Poisson's ratio	Density (kg/m <sup>3</sup> )	Piezoelectric
		Modulus (GPa)			voltage constants (C/m <sup>2</sup> )
Aluminium	/	69	0.3	2700	/
Brass	/	110	0.3	6400	/
PZT4	$\begin{bmatrix} 804.6 & 0 & 0 \\ 0 & 804.6 & 0 \\ 0 & 0 & 659.7 \end{bmatrix}$	$\begin{bmatrix} 132 & 71 & 73 & 0 & 0 & 0 \\ & 132 & 73 & 0 & 0 & 0 \\ & & 115 & 0 & 0 & 0 \\ & & & 30 & 0 & 0 \\ & & & & 26 & 0 \\ & & & & & 26 \end{bmatrix}$	/	7500	$\begin{bmatrix} 0 & 0 & -4.1 \\ 0 & 0 & -4.1 \\ 0 & 0 & 14.1 \\ 0 & 0 & 0 \\ 0 & 10.5 & 0 \\ 10.5 & 0 & 0 \end{bmatrix}$

### 3.2 The squeeze film model of the actuator

The infinite-width squeeze film governing equations for a fixed floating object consist of the Reynolds equation and the film thickness equation as defined by the shapes of the plate at a specific frequency. Due to the dimension of the exciting plate and the actual form of a conveyor, it is reasonable to calculate with an infinite-width mode.

The film thickness equations with pure flexural modes are shown in Fig.4.

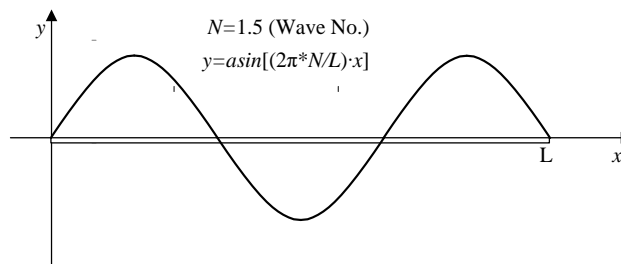


Fig.4 Theoretical model of the squeeze film

Where,  $N$  is wave number, which means the number of wavelength in the exciting plate.  $Y$  is the modal shapes equation in order to determine the position of the vibration point.

So, the dimensionless governing equations for the infinite width plate are listed as follows:

The dimensionless film thickness equation:

$$H(X,T) = 1 - Y(X) \cdot \sin T \dots\dots\dots 1$$

And the Reynolds equation:

$$\frac{\partial}{\partial X} \left( PH^3 \frac{\partial P}{\partial X} \right) = \sigma \frac{\partial(PH)}{\partial T} \dots\dots\dots 2$$

Where, the dimensionless parameters  $H = \frac{h}{h_0}$ ,  $X = \frac{x}{L} \in (0, 1)$ ,  $P = \frac{p}{p_a}$ ,  $T = \omega t$ ,  $\sigma = \frac{12\mu\omega b^2}{h_0^2 p_a}$  (squeeze number),

$$Y(X) = a \cdot \sin(2\pi N \cdot X) / h_0$$

For the square sample, the bearing force can be derived by the pressure integral, as follows

$$f_1(T) = \iint_{S_1} (p - p_a) dx dy = \int_0^a \int_0^b (p - p_a) dx dy \dots\dots\dots 3$$

Where,  $S_1$  is the square integral area;  $a$ ,  $b$  are the length and the width respectively.

For the round sample, the pressure integral can be derived as

$$f_2(T) = \iint_{S_2} (p - p_a) r dr d\theta = \int_0^{R_0} \int_0^{2\pi} (p - p_a) r dr d\theta \dots\dots\dots 4$$

Where,  $S_2$  is the round integral area;  $R_0$  is the radial of the sample;  $x = r \cos\theta$ ,  $y = r \sin\theta$ .

The program flow chart is shown as Fig.5. The Reynolds equation was calculated by the means of centre difference and coupled with the film thickness equation including the plate deformation.

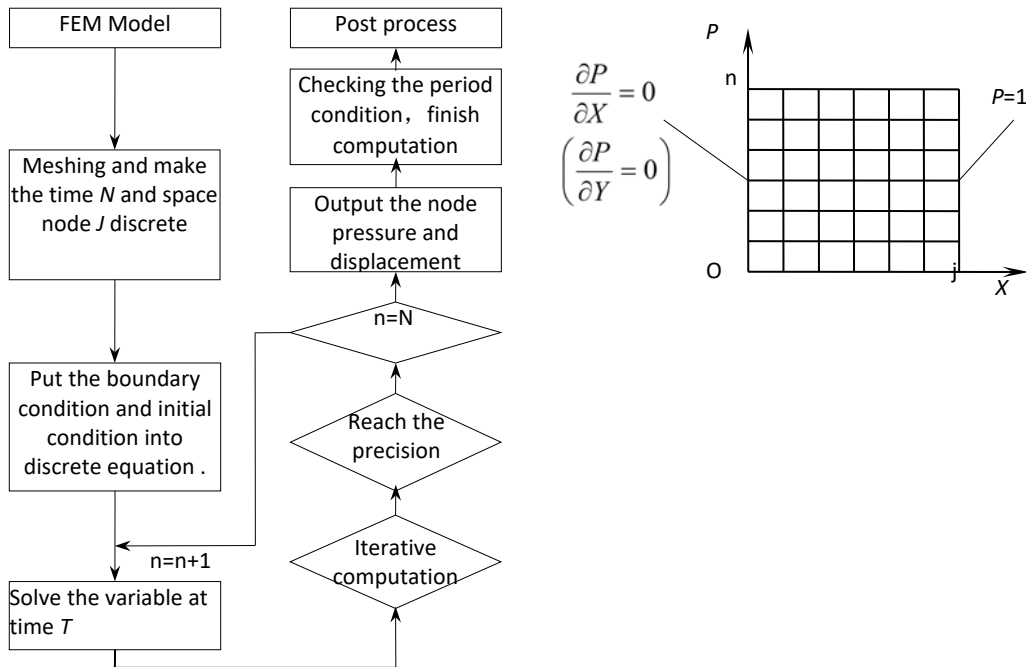
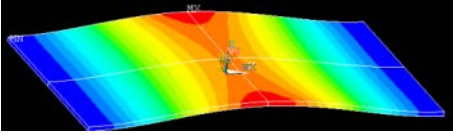
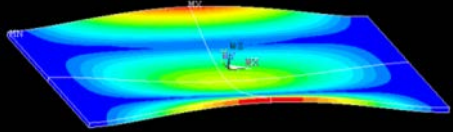
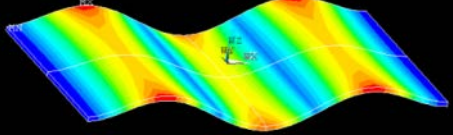
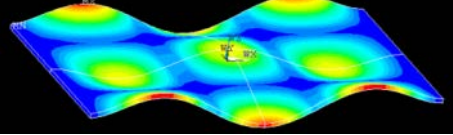
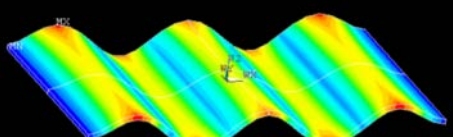


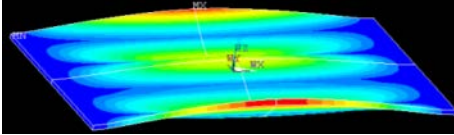
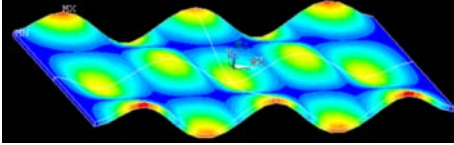
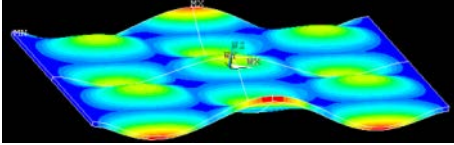
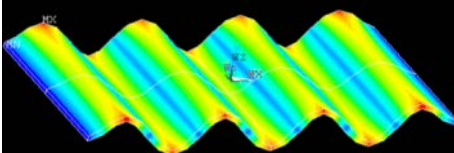
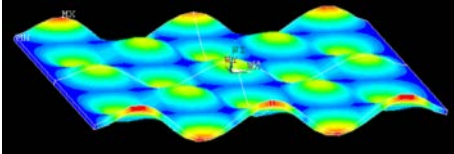
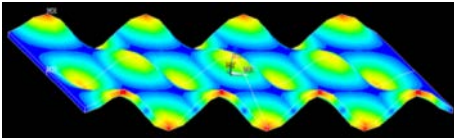
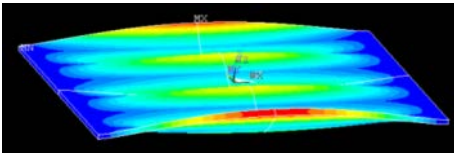
Fig.5 flowchart of the theoretical solving

## 4 Results and discussion

The modal shapes calculated by ANSYS are listed in Tab.5 (below 15 kHz). The symmetry model can explain the basic forms for the exciting plate. There are three kinds of modal shapes. First, they are the pure flexural mode along  $X$  direction such as Mode 1st, 3rd, 5th and so on. Second, they are the pure flexural modes along  $Y$  direction such as 2nd, 6th, 12th, and so on. The last are mixed wave shapes with different wave number along  $X$  and  $Y$  direction. For example, the fourth step of modal shapes show the  $1.5 \times 1$  mixed wave shapes.

Tab.5 The ANSYS simulated modal shapes of the exciting plate

Model	Images	Explanation
Frequency	Expanded from the $\frac{1}{4}$ model	
1(417.9)		Pure flexural wave along $x$ direction
2(1461.8)		Pure flexural wave along $y$ direction
3(2291.3)		Pure flexural wave along $x$ direction
4(3632.0)		Mixed modal with both $x$ and $y$ direction( $1.5 \times 1$ )
5(5794.0)		Pure flexural wave along $x$

6(6124.5)		Pure flexural wave along y
7(7274.8)		Mixed modal with both x and y direction(2.5*1)
8(8202.4)		Mixed modal with both x and y direction(2*1.5)
9(11128.9)		Pure flexural wave along x
10(11994.3)		Mixed modal with both x and y direction(2.5*2.5)
Not addressed in experiments: (12662.9)		Mixed modal with both x and y direction(3.5*2)
11(14853.8)		Pure flexural wave along y

---

For an effective conveyor, the larger amplitude in the central line of the plate is needed. The forced harmonic spectrum at the origin point (central point) is shown as Fig. 6. Not all of the modes can be simulated well in the forced vibrating condition and also, not all of the peaks of vibrating amplitude are the natural modes, but some are the harmonic modes. The amplitude-frequency curves show the magnitude trend with the increase of the frequency. Nearly all the modal shapes can be excited but with different magnitudes. The harmonic results correspond to the modal shapes but the resonant frequency is different, due partially to the coupling effect of piezo-electric materials.

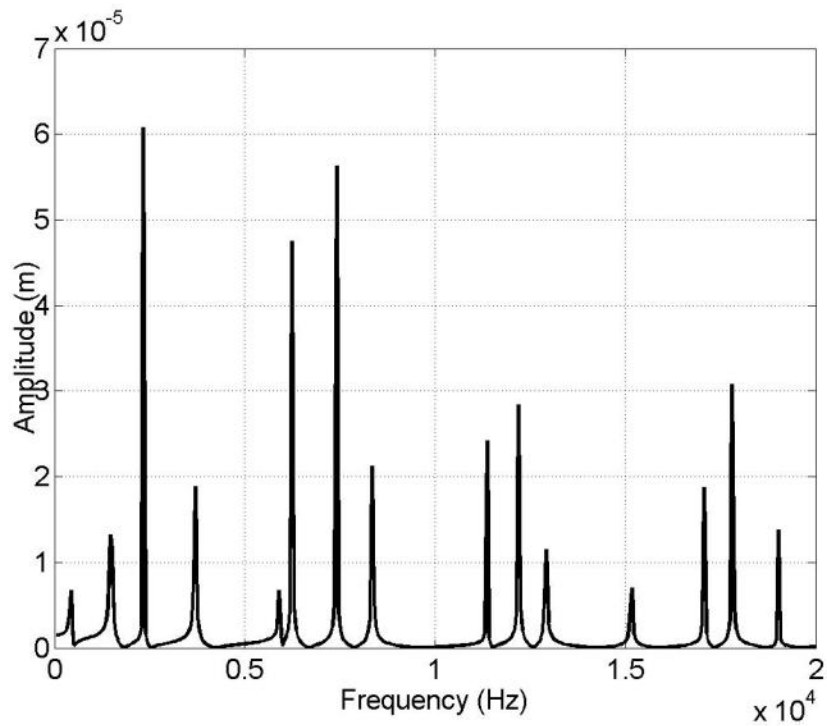


Fig.6 Harmonic analysis results at central point

## 5 Experiments and verification

The experimental arrangement is shown in Fig.7, including signal generator, power supply amplifier, oscilloscope, capacitive sensor (accumulator) and multimeter. Some key parameters in the experiments are listed in Tab.6.

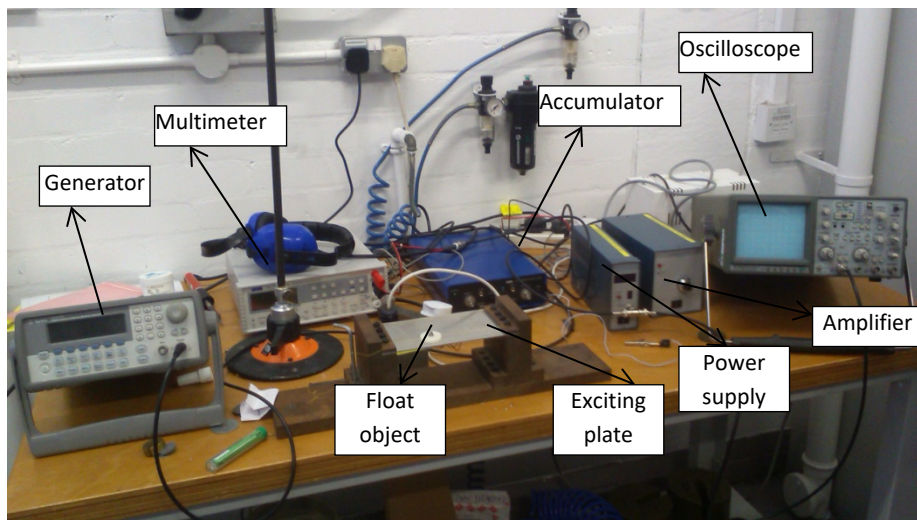


Fig.7 The layout of the experiments

Tab.6 The Experiment parameters

Bandwidth:	Acquisition	Sample	Frequency	Frequency
	Mode:	frequency:	Resolution:	Range:
50 kHz	FFT	128 kHz	1.95 Hz	75 V

The harmonic shapes of the plate were measured by a laser scanning vibrometer from the Polytec Company. 41x25 total 1025 nodes are distributed on the plate to collect the velocity on Z (height) direction as Fig.8. The sweeping voltage input to the amplifier was 5V AC, generating an amplifier output of 75V AC.

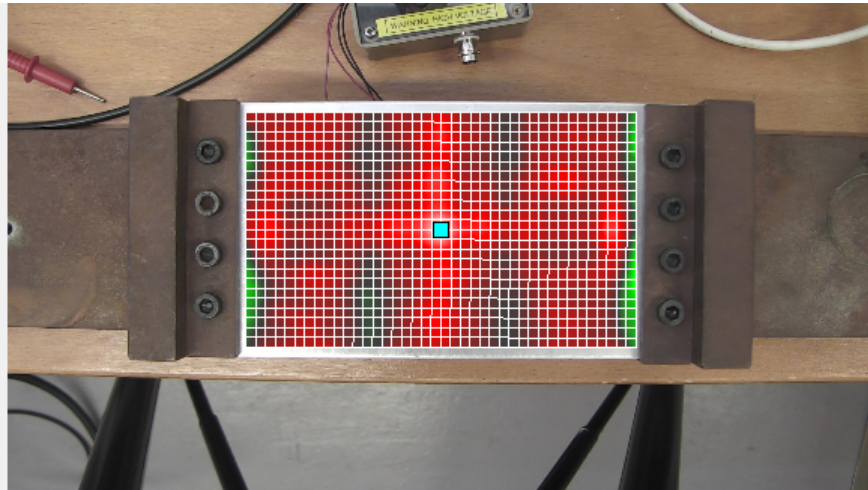


Fig.8 The laser scanning vibrometer mesh grid for the modal test

The average RMS velocity on all surface nodes curves versus frequency is shown in Fig.9. In contrast to the symmetry modes in ANSYS, some of the harmonic resonance of the plate could be missing and the peaks are more irregular. The best levitation frequencies and modal shapes are identifiable in the spectrum. The harmonic shapes are measured below 15 kHz frequency from the experiments and the corresponding plate deformations are listed in Tab.7.

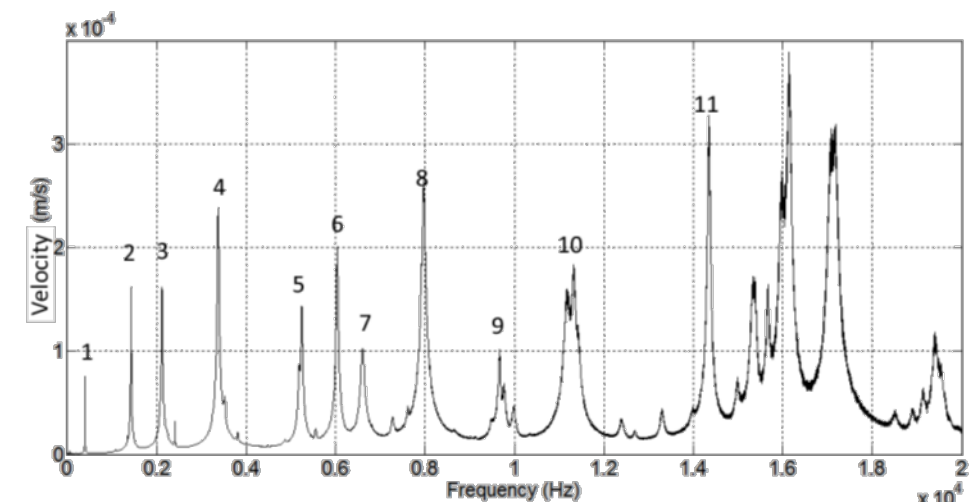
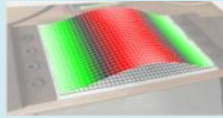
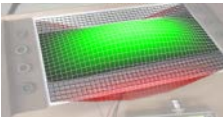
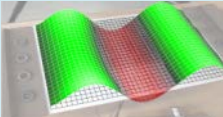
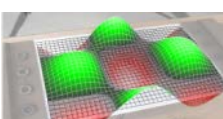
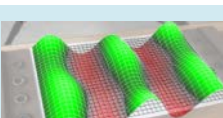
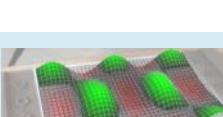
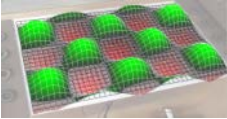
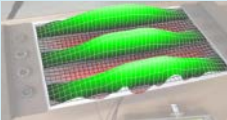


Fig.9 Average velocity values of experimental data

Tab.7 the experiment results measured by Polytec laser scanning vibrometer

Sequence	Frequency	Harmonica shapes	Magnitude ( $\mu\text{m}$ )	Theoretical errors	Floating
1	393.7		75.12	5.8%	unavailable
2	1425.0		161.4	2.5%	available
3	2115.6		162.03	7.7%	available
4	3671.9		238.65	1.1%	unavailable
5	5240.6		143.04	9.5%	unavailable
6	6037.5		200.8	1.4%	unavailable
7	6612.5		102.35	9.1%	available
8	7965.6		264.42	2.9%	available
9	9668.8		101.19	13.1%	unavailable

10	11178.1		160.11	6.8%	available
11	14353.1		327.84	3.3%	unavailable

Comparing the simulation results in Tab.5, with the experimental results in Tab.7, we find that the symmetry model can better predict the modal shape of the plates. All of the theoretical shapes of peaks are included in the Tab.5 for frequencies below 15 kHz. The theoretical errors for all the simulation results are below 15%. The largest errors occur along the X direction (step 3, 5, 9) due to the simplified boundary condition. In contrast, the errors along Y direction have better accuracy due to the free boundaries. The experiment results show that not all of the modal shapes produce object self-levitation. The pure modes are appropriate for lower frequency while the mixed modes are appropriate for higher frequency. This phenomenon can explain why some researchers have different optimisation modal shapes for the self-levitation of different structures and this result provides significant guidance to prototype design.

The results for displacement of the central point are shown in Fig.10. It is different to the RMS curves but has a similar trend. By contrast with the harmonic simulation results (Fig.6), the results imply that the amplitude of the central point represents the whole vibrating status to a certain extent.

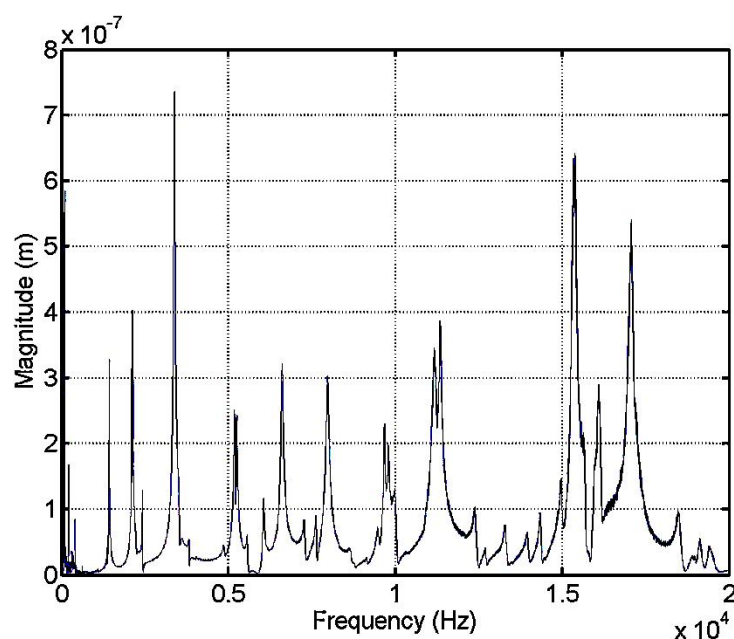


Fig.10 the experiment results of the central point

The levitation experiment needs a more powerful amplifier to enlarge the energy input. The performance parameters of the Fuji amplifier are listed as Tab.8. It provides a fixed 15 times gain for all D.C and A.C signal inputs. Its working point can be adjusted for obtaining the largest bandwidth for the experiments. The levitation height of the object was measured by the laser scanning vibrometer (Fig.11). The levitation object shown is made of nylon with dimensions  $\Phi 25\text{mm} \times 3\text{mm}$  and a mass of 6g. For the largest energy output, the working point should be adjusted in the amplifier. The 7 volt offset (before amplification) generated the largest amplitude and avoided clipping as observed on the oscilloscope.

Tab.8 Performance parameters of the Fuji amplifier and power supply.

Performance index	Range
Output Voltage	0-150V
Output Current	1A
Voltage range	0-+150V
Bandwidth	DC-100KHz (100V <sub>p-p</sub> output)
Internal resistance	100KΩ
Amplification	25 dB(15 times)
The Stability to time	$1 \cdot 10^{-4}/h$
The Stability to Current	$1 \cdot 10^{-4}$
Dimension	103mm(W)*124mm(H)*220mm(D)
Weight	4.5Kg

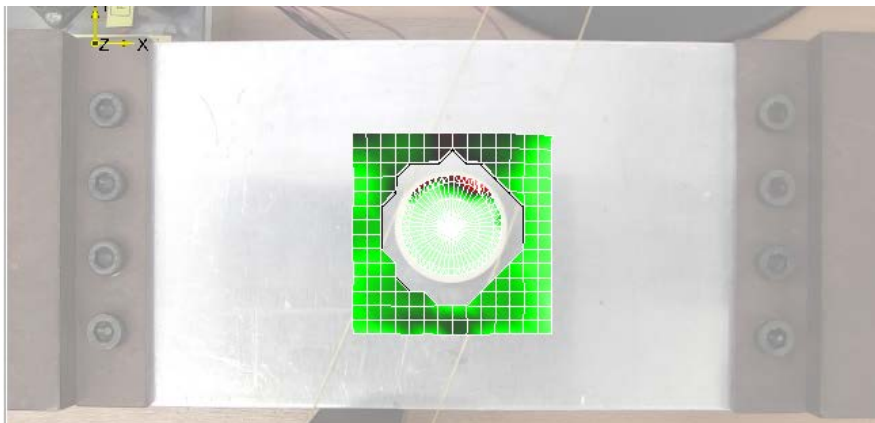


Fig.11 Mesh grid for the levitation height of the object measurement

The levitation experiment results and fitted curves are shown in Fig.12. All the experiment points correspond to the modal results in Tab.7 (Black Square). The results show that the levitation can be achieved at 6 points in the frequency band, whilst other points fail to levitate. The levitation points show that the pure flexible wave is appropriate for

achieving levitation at low frequency and the mixed shapes are appropriate for levitation at higher frequencies. This finding can guide and optimize the design of NFAL platform to work in different frequency bands.

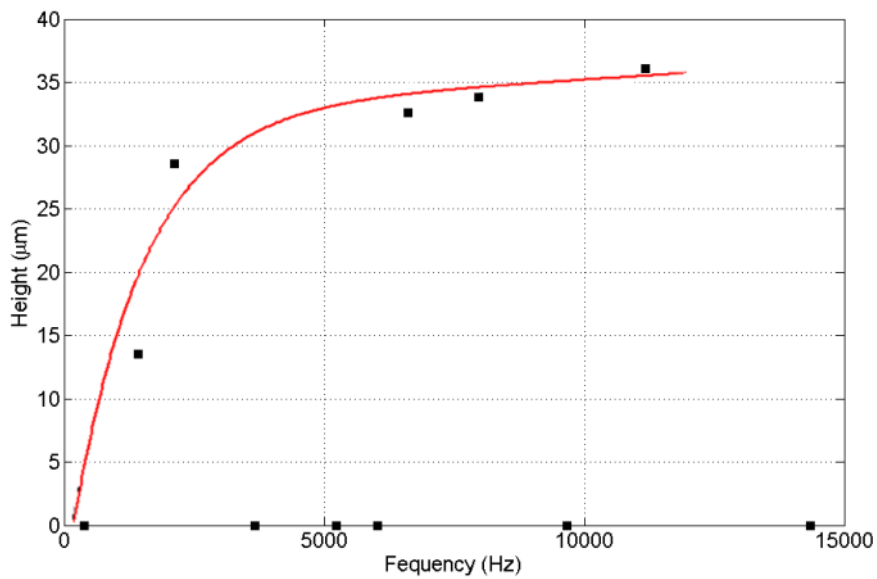


Fig.12 The levitation experiment results

The fitted curve is an exponential function with 95% confidence bounds:

$$F(x)=32.2*\exp(8.416e-6*x) -44.86*\exp(-7.764e-4*x).....4$$

This equation can provide an estimated levitation height of the object, the trend of the levitation curve is reasonable and corresponds to the theoretical results [7], [20] and is comparable with experimental results reported by Atherton et al [21].

## 6 Conclusion

- 1) The plate actuator with four piezo-electric discs has significant load-bearing force that can be used for the conveying of objects.
- 2) Almost all of harmonic shapes can be expressed by one-quarter simulation models. The symmetry shapes have larger load-bearing capacity and the levitated object is more stable.
- 3) The most appropriate mode is determined by the range of working frequencies, for the lower band, pure flexural modes are appropriate and the mixed modes are better for higher frequencies.

- 4) For acquiring more energy from the amplifier, the working point should be set up to guarantee the largest amplitude and avoiding amplifier clipping.
- 5) The levitation height is an exponential function of frequency in general, which is consistent with theoretical results.

## References

---

- [1]Gross, W.A., (1962). Gas Film Lubrication, New York :Wiley.
- [2]Langlois, W.E., (1962). Isothermal Squeeze Films, Quarterly of Applied Mathematics. 1962.XX(2), pp 131-150.
- [3]Salbu, E.O.J., (1964). Compressible squeeze films and squeeze bearings ASME J of Basic Eng 86(3), pp 355-366.
- [4]Beck, J.V., Holliday, W.G., Strodman, C.L., (1969). Experiment and analysis of a flat disk squeeze-film bearing including effects of supported mass motion. ASME J of Lubrication Technology,91(1), pp 138-148
- [5]Kuroda, S., N. Hirata. (1984). The Characteristics of Motion of a Round Plate Supported on Squeeze Air Film." *Trans. Jpn. Soc. Mech. Eng., Ser. B* 50.459, pp 2727-2731.
- [6]Jing, M.Q., Liu, H., Shen, Y., Yu, L., (2008). New Style Squeeze Film Air Bearing. Journal of Xi'an Jiaotong University, 42(07), pp 799-802.
- [7]Hashimoto, Y., Koike, Y., Ueha, S., (1996). Near field acoustic levitation of planar specimens using flexural vibration. J. Acoust.Soc. America, 100(4), pp 2057-2061.
- [8]Minikes, A., Bucher, I., (2004). Levitation force induced by pressure radiation in gas squeeze films. J.Acoust.Soc America, 116(1), pp 217-226.
- [9]Stolarski, T.A., Chai, W., (2006). Load-carrying capacity generation in squeeze film action. International Journal of Mechanical Sciences. 48(7), pp 736–741.
- [10]Stolarski, T.A., (2010). Numerical modelling and experimental verification of compressible squeeze film pressure. Tribology International. 43(1), pp 356-360.
- [11]Liu, P., Li, J., Ding, H., (2009). Modeling and experimental study on Near-Field Acoustic Levitation by flexural mode, IEEE Trans. Ultrason. Ferroelectr. Freq.Control. 56(12), pp 2679-2685.
- [12]Li, J., Liu, P., Ding, H., Cao, W., (2011). Modeling characterization and optimization design for PZT transducer used in Near Field Acoustic Levitation. Sensors and Actuators A. 171(2), pp 260–265.
- [13]Wei, B., Ma, X., (2010). Research on the Characteristic of the Floating Guide Way with Squeeze Film., Lubrication Engineering, 35(8), pp 54-58.
- [14]Wei, B., Ma, X., (2010). Research on the Characteristics of Squeeze Film Floating Guide Way Including the Model Effect. Lubrication Engineering, 35(2), pp 33-35.
- [15]Li, J., Cao, W., Liu, P., Ding, H., (2010). Influence of gas inertia and edge effect on squeeze film in near field acoustic levitation. Appl. Phys. Lett. 96(24), 243507 pp 1-8.
- [16]Xie, W.J., Wei, B., (2012). Parametric study of single-axis acoustic levitation. Appl. Phys. Lett. 79(4), pp 881-886.
- [17]Nabhani, M., El-Khlifi, M., , Bou-Said, B., (2012). Combined Non-Newtonian and viscous shear effects on porous squeeze film behavior. Tribology Transactions, 55(4), pp 491-502.
- [18]Rao, T., Rani, A.M.A., Nagarajan, T., (2013). Analysis of journal bearing with double-Layer porous lubricant film: Influence of surface porous layer configuration. Tribology Transactions, 56(5), pp 841-847.
- [19]Bouزيدane, A. Thomas, M., (2013). Nonlinear dynamic analysis of a rigid rotor supported by a three-pad hydrostatic squeeze film dampers. Tribology Transactions. 56(5), pp 717-727.
- [20]Wang, Y.Z., Wei, B., (2013). Mixed-modal disk gas squeeze film theoretical and experimental analysis. International Journal of Modern Physics. 27(25), 1350168, pp 1-20.
- [21]Ha, D.N.; Stolarski, T.A.; Yoshimoto, S. (2005). An aerodynamic bearing with adjustable geometry and self-lifting capacity. Part 1: self-lift capacity by squeeze film. Proc. Institution of Mechanical Engineers, Part J: Journal of Engineering Tribology, , 219(J1), pp 33-39.
- [22]Wang, Y.Z., Wei, B., (2013). A linear solution for gas squeeze film characteristics in ultrasonic excitation condition. The Journal of the Chinese Society of Mechanical Engineers, 34(5), pp 469-473.
- [31] Atherton, M.A., Mares, C., Stolrski, T.A., (2014). Some fundamental aspects of self-levitating sliding contact bearings and their practical implementations. Proc. Institution of Mechanical Engineers, Part J: Journal of Engineering Tribology, 228(9), pp 916-927.

## Nomenclature

$y$ (m)	The width of plate actuator	$L$ (m)	Width Variable
$Y$	The dimensionless form of $y$	$p$ (pa)	Squeeze film pressure
$t$ (s)	Time	$p_0$ (Pa)	Atmospheric Pressure
$T$	The dimensionless form of $t$ $T = \omega t$	$P$	The dimensionless form of $p$ $P = p/p_0$
$m$ (kg)	The mass of free levitation object	$h_0$ (m)	Initial film thickness
$f$	Squeeze frequency	$\omega$ (rad/s)	Squeezing angular frequency $\omega = 2\pi f$
$\mu$ (pa·s)	Dynamic viscosity	$g$ (N)	Bearing force
$\sigma$	Squeeze Number $\sigma = \frac{12\mu\omega b^2}{h_0^2 p_a}$	$F$	Dimensionless bearing force $F(T) = \frac{g(T)}{p_0 R_0^2}$
$h$ (m)	Film Thickness	$X$	The dimensionless form of $x$ $X = x/L$
$H$	The dimensionless form of $h$ $H = h/h_0$		

## Appendix

### 1 The dimensionless film thickness equation derivation for plate actuator

The equation of wave shape in the coordinate in Fig.4 is

$$y = a \cdot \sin[(2\pi \cdot N/L) \cdot x]$$

Where,  $a$  is the amplitude of the plate shape,  $N$  is the wave number,  $L$  is the length of the plate,  $x$  is the position of the vibrating point.

Then, the film thickness equation is derived as

$$h = h_0 - y(x) = h_0 - a \cdot \sin[(2\pi \cdot N/L) \cdot x]$$

Where,  $h_0$  is the initial film thickness,  $h$  is the simultaneous film thickness.

Use  $Y = y/h_0$ ,  $X = x/L$ ,  $H = h/h_0$  to derive the dimensionless equations as follows

$$H = 1 - Y(X) = 1 - a \cdot \sin(2\pi N \cdot X) / h_0$$

### 2 Governing equations of different squeeze film models for disc actuator

#### 1) Fixed object (wall)

Dimensionless film thickness equation:

$$H = 1 - \epsilon \cos T$$

Dimensionless Reynolds equation  $\frac{H^3}{R} \frac{\partial}{\partial R} (R P \frac{\partial P}{\partial R}) = \sigma \frac{\partial (P H)}{\partial T}$

$$\text{Where, } \sigma = \frac{12\mu\omega R_0^2}{p_0 h_0^2}; \quad P = \frac{p}{p_0}; \quad R = \frac{r}{R_0}; \quad T = \omega t; \quad H = \frac{h}{h_0}$$

#### 2) Free object levitation

Dimension film thickness equation:

$$H = 1 - \epsilon \cos T + Y$$

---

Where,  $y = h_0 Y$ ,  $T = \omega t$ ,  $h = h_0 H$ ,  $\varepsilon = \delta h / h_0$

Dimensionless motion equation:

$$\frac{d^2 Y}{dT^2} = \alpha \left( 2 \int_0^1 PR dR - 1 - W \right)$$

Where,  $\alpha = \frac{\pi p_a R_0^2}{m \omega^2 h_0}$ ,  $W = \frac{w}{\pi R_0^2 p_a}$ ,  $Y = \frac{y}{h_0}$ ,  $T = \omega t$ ,  $P = \frac{p}{p_a}$ ,  $R = \frac{r}{R_0}$

### 3) Ideal flexuous wave exciting

Dimension film thickness equation:

$$H = (1 - \varepsilon \cos - kR) + Y$$

Where,  $y = h_0 Y$ ,  $T = \omega t$ ,  $h = h_0 H$ ,  $\varepsilon = \delta h / h_0$ ,  $\Lambda = \lambda / 2R_0$  (dimensionless wave length),  $k = 2\pi / \Lambda$  Dimensionless

motion equation

$$\frac{d^2 Y}{dT^2} = \alpha \left( 2 \int_0^1 PR dR - 1 - W \right)$$

Where,  $\alpha = \frac{\pi p_a R_0^2}{m \omega^2 h_0}$ ,  $W = \frac{w}{\pi R_0^2 p_a}$ ,  $Y = \frac{y}{h_0}$ ,  $T = \omega t$ ,  $P = \frac{p}{p_a}$ ,  $R = \frac{r}{R_0}$

Dimensionless Reynolds equation  $\frac{1}{R} \frac{\partial}{\partial R} \left( H^3 R P \frac{\partial P}{\partial R} \right) = \sigma \frac{\partial (PH)}{\partial T}$